

# Metal Dicyanamides as Efficient and Robust Water-Oxidation Catalysts

Satya Vijaya Kumar Nune,<sup>[a]</sup> Aysun Tekin Basaran,<sup>[a]</sup> Emine Ülker,<sup>[a, b]</sup> Rupali Mishra,<sup>[a]</sup> and Ferdi Karadas<sup>\*[a, c]</sup>

Non-oxide cobalt-based water-oxidation electrocatalysts have received attention recently for their relative ease of preparation, they are stable both in acidic and basic media, and they have higher turnover frequencies than cobalt oxides. Recent studies show that one of the main bottlenecks in the implementation of non-oxide systems to water splitting is the low number of active metal sites, which is in the order of  $\text{nmol cm}^{-2}$ . Herein, a new series of non-oxide water-oxidation catalysts has been introduced to the field. Cobalt dicyanamides

are observed to have around four times higher surface active sites and better catalytic performances than cyanide-based systems. Long-term catalytic studies (70 h) at an applied potential of 1.2 V and electrochemical studies performed in solutions in pH values of 3.0–12.0 indicate that the compounds are robust and retain their structures even under harsh conditions. Moreover, the addition of Ni impurities to cobalt dicyanamides is a feasible method to improve their catalytic activities.

## Introduction

Fossil-based fuels have been used extensively for centuries, but the reserves of these fuels are being depleted rapidly.<sup>[1]</sup> Moreover, the use of these fuels has a serious impact on the environment, such as hazardous greenhouse gas emissions and the change in the atmospheric equilibrium,<sup>[2]</sup> which emphasizes the necessity for more reliable, clean, and environmental friendly power sources.<sup>[3]</sup> Given the high energy density of hydrogen ( $143.0 \text{ MJ kg}^{-1}$ ), hydrogen-based fuels are one of the most promising alternatives<sup>[4]</sup> for clean and renewable energy without any waste.<sup>[5]</sup> Water splitting, which involves the production of  $\text{H}_2$  and  $\text{O}_2$  from water, is considered to be the bottleneck in the hydrogen economy.<sup>[6]</sup> The conversion of solar energy into chemical energy through the splitting of water molecules in photosynthesis is a well-defined process that uses chlorophyll. The whole procedure works on the association of an electron acceptor and an electron donor.<sup>[7]</sup>

Over the past few decades, many research groups have aimed to perfect the art of mimicking the photosynthesis process of splitting water to generate energy.<sup>[8]</sup> Both electrocatalytic<sup>[9]</sup> and photocatalytic<sup>[10]</sup> routes have been studied extensively with a wide range of catalysts, which include semiconductors,<sup>[11]</sup> transition metal oxides,<sup>[12]</sup> metal–organic frameworks (MOFs),<sup>[13]</sup> perovskite-type compounds,<sup>[14]</sup> and amorphous and porous catalysts.<sup>[15]</sup> Over the past few years, non-oxide systems have been emphasized not only because of their high stabilities in both acidic and basic media but also because of their high catalytic activities obtained per metal site. Various Co-based non-oxide systems such as cyanide,<sup>[16]</sup> and cyanamide-based systems<sup>[17]</sup> are efficient and robust water-oxidation catalysts (WOCs). In 2014, Galán-Mascarós et al. reported the application of various metal hexacyanometalates as heterogeneous WOCs, which are stable even under extremely acidic conditions and had quantum yields in the range 50–80%.<sup>[16a]</sup> A similar study was reported in 2015 by Fukuzumi et al. who used hetero-polynuclear cyanide systems with Co and Pt ions.<sup>[18]</sup> In 2016, the use of pentacyanoferrate-coordinated poly(4-vinylpyridine) as a precursor to obtain a cyanide-based coordination polymer with a high current density at low overpotentials was reported by our group.<sup>[19]</sup> Furthermore, Patzke et al. reported the application of cobalt carbodiimide for both photochemical and electrochemical water oxidation in neutral and basic media in 2015.<sup>[17]</sup> Overall, these studies suggest that heterogeneous WOCs with Co ions exhibit excellent turnover frequencies (TOFs) if the metal ions are surrounded by N donor atoms rather than O atoms as in the case of oxides. The electrocatalytic studies performed on homogeneous single-site WOCs,  $[\text{Co}(\text{Py}5)(\text{OH}_2)](\text{ClO}_4)_2$  ( $\text{Py}5 = 2,6$ -[bis(bis-2-pyridyl)-methoxymethane]pyridine)<sup>[20]</sup> and cobalt

[a] Dr. S. V. K. Nune, A. T. Basaran, Prof. Dr. E. Ülker, Dr. R. Mishra, Prof. Dr. F. Karadas  
Department of Chemistry  
Bilkent University  
06800, Ankara (Turkey)  
E-mail: karadas@fen.bilkent.edu.tr

[b] Prof. Dr. E. Ülker  
Department of Chemistry, Faculty of Arts & Sciences  
Recep Tayyip Erdogan University  
53100, Rize (Turkey)

[c] Prof. Dr. F. Karadas  
UNAM-Institute of Materials Science and Nanotechnology  
Bilkent University  
Ankara, 06800 (Turkey)

Supporting information and the ORCID identification number(s) for the author(s) of this article can be found under <http://dx.doi.org/10.1002/cctc.201600976>.

hangman porphyrins,<sup>[9a]</sup> which involve single Co atoms surrounded by N donor atoms, also support this.

In our current investigation, we are interested in expanding the portfolio of heterogeneous WOCs that contain metal ions surrounded by N donor atoms. The type of ligand plays a critical role in the stability and the catalytic performance of the compounds. Our current research focuses on the introduction of a new N-donor bridging group, dicyanamide ( $\text{N}(\text{CN})_2^-$ ), to this field. Metal dicyanamide systems have been explored to a great extent for their interesting structures,<sup>[21]</sup> magnetic properties,<sup>[22]</sup> and selectivity in gas adsorption.<sup>[23]</sup> For the first time, we report the application of a cobalt dicyanamide matrix in electrochemical WOCs. Moreover, a 1D coordination compound rather than a 3D extended network was chosen as a catalyst of interest to improve the number of active metal sites as the main drawback of non-oxide Co-containing WOCs is the relatively low number of active metal sites on the surface because of the larger distance between the metal sites compared to that in oxide-based systems.

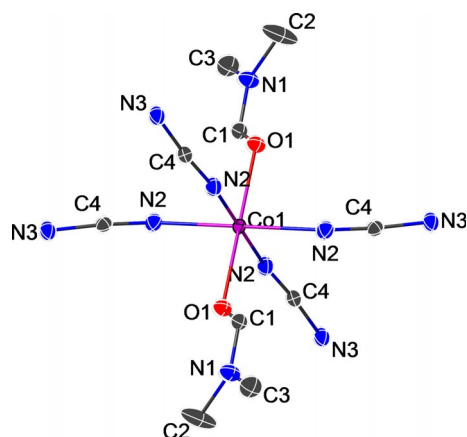


**Figure 1.** Fragment of the crystal structure of  $\text{Co}(\text{dca})_2(\text{dmf})_2$ , which depicts the  $\text{MN}_4\text{O}_2$  coordination sphere of the metal site. Thermal ellipsoids are projected at the 50% probability level. Hydrogen atoms are not shown for clarity.

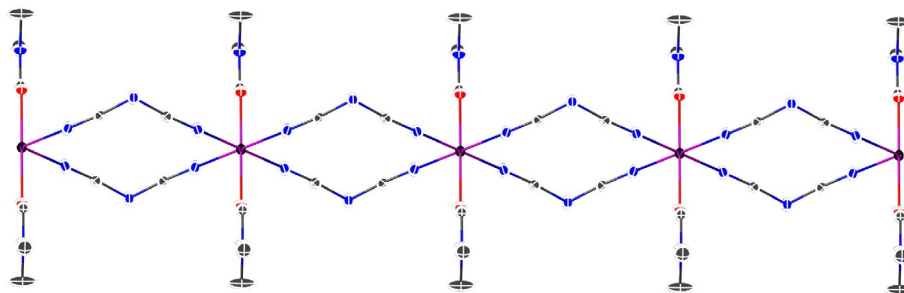


**Figure 2.** 1D chain structure of  $[\text{Cocda}2]$ . Color code: Co = purple; O = red; C = gray; N = blue. Thermal ellipsoids are projected at the 50% probability level. Hydrogen atoms are not shown for clarity.

## Results and Discussion

### Synthesis and characterization

Single-crystal XRD studies performed on fine crystals of the compounds reveal that they are all isostructural and crystallize in a monoclinic system with the space group  $P21/n$ . The crystallographic structure and refinement parameters are given in Table S1. The asymmetric unit of the  $\text{M}(\text{dca})_2$  (DCA = dicyanamide) structure contains half of a metal(II) site, two dicyanamide groups, and one DMF molecule. Each metal ion shows a distorted octahedral  $\text{MN}_4\text{O}_2$  coordination environment, which results from the coordination of four N atoms of different DCA groups and two O atoms from DMF molecules (Figure 1). The crystal structure could be described as a 1D ladder-like double-chain coordination polymer (Figure 2). Neighboring metal ions in each chain are connected to each other through two dicyanamide groups, which results in a distance of 7.3 Å between the  $\text{Co}^{\text{II}}$  centers. Two ligands adopt a certain configuration to connect two metal centers in such a way as to form rectangular units. All of the M–N and M–O distances are within the normal range of statistical errors (Table S2). The supramolecular framework is stabilized by  $\text{H}\cdots\text{N}$  interactions (2.555(5)–2.686(5) Å), which originate from the H atoms of the coordinated DMF molecules and the central N atom of the DCA groups (Figure S1 and S2).

Powder XRD studies of the as-synthesized metal dicyanamide clusters (Co, Fe, and Ni) confirm that the series of compounds is isostructural with varying degrees of crystallinity. The XRD patterns, which exhibit  $2\theta$  positions that almost overlap each other, are presented in Figure 3.

The IR spectra of the Co and Ni derivatives exhibit sharp and strong stretching bands, whereas that of the Fe cluster shows broad and weak bands (Figure 4). The  $\nu_{\text{sym}\&\text{asym}}(\text{C}\equiv\text{N})$  stretches were observed in the range  $\tilde{\nu} = 2360\text{--}2184\text{ cm}^{-1}$ , the  $\nu_{\text{asym}}(\text{C}\text{--}\text{N})$  stretch was at around  $\tilde{\nu} = 1380\text{--}1364\text{ cm}^{-1}$ , and the  $\nu_{\text{sym}}(\text{C}\text{--}\text{N})$  stretch was at around  $\tilde{\nu} = 938\text{ cm}^{-1}$ , all of which can be attributed to the cyanide groups in the DCA fragments.<sup>[23a]</sup> Strong bands at  $\tilde{\nu} = 1108\text{--}1015\text{ cm}^{-1}$  correspond to the C–N group, whereas bands at around  $\tilde{\nu} = 1647\text{--}1640$  and  $2970\text{--}2934\text{ cm}^{-1}$  can be assigned to the C=O stretches and aliphatic C–H stretching vibrations of DMF, respectively.<sup>[24]</sup> The presence of a broad stretch at  $\tilde{\nu} = 3500\text{--}3250\text{ cm}^{-1}$  in the spectrum of

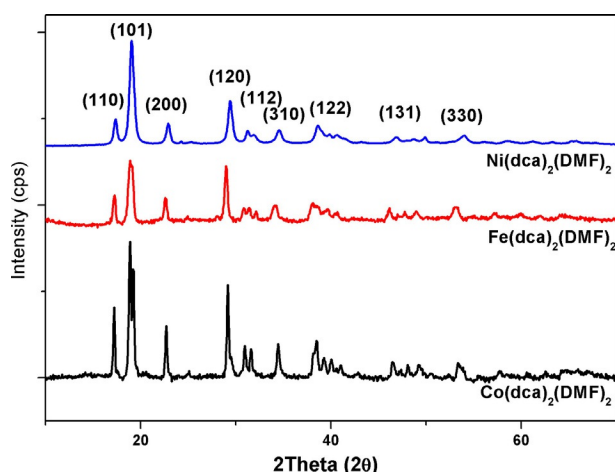


Figure 3. XRD patterns of [Mdca2].

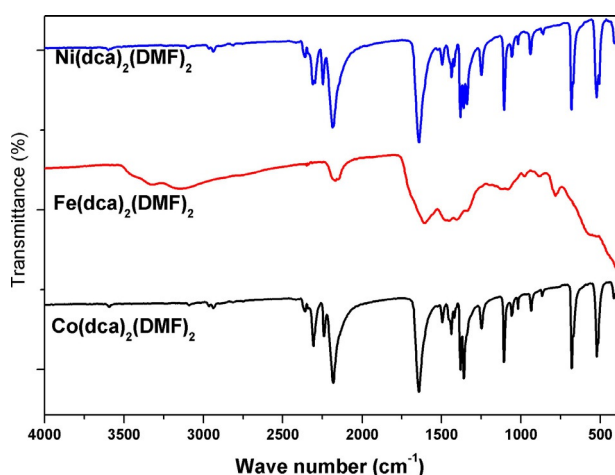


Figure 4. FTIR spectra of [Mdca2].

the Fe derivative can be caused by the adsorption of excess moisture, which can also be a reason for the relatively poor crystallinity of the Fe derivative.

### Electrochemical studies

Cyclic voltammograms (CVs) of  $M(\text{dca})_2(\text{dmf})_2$  ( $M = \text{Co}, \text{Fe},$  and  $\text{Ni}$ ) deposited on fluorine-doped tin oxide (FTO) electrodes, referred to as [Mdca2] henceforth, were recorded in a phosphate buffer solution with 1 M  $\text{KNO}_3$  as the electrolyte over 0–1.5 V vs. Ag/AgCl (Figure 5). The prominent feature of the CVs of [Mdca2] is the increase in the anodic current above  $\sim 1$  V, which can be attributed to catalytic oxygen evolution. The CVs of the three derivatives reveal that [Codca2] shows a significantly higher catalytic activity than the Fe and Ni derivatives. Hence further studies were performed with [Codca2]. The CV of [Codca2] shows a quasireversible redox couple with a significant oxidation peak at 0.95 V and a reduction peak at 0.83 V vs. Ag/AgCl ( $E_{1/2} = 0.89$  V,  $E_c - E_a = 120$  mV), which can be assigned to the  $\text{Co}^{2+}/\text{Co}^{3+}$  redox couple. A second oxidation pro-

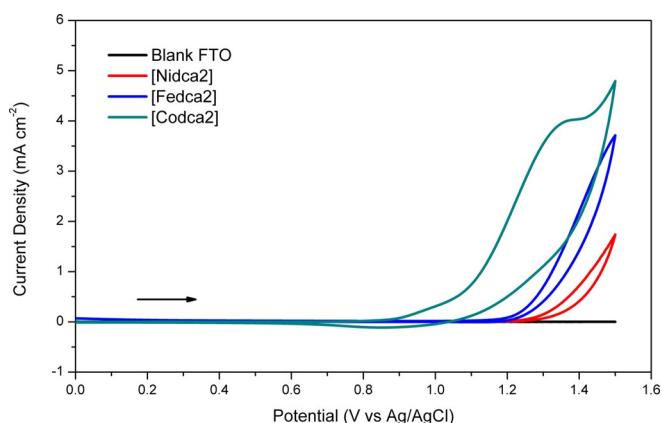
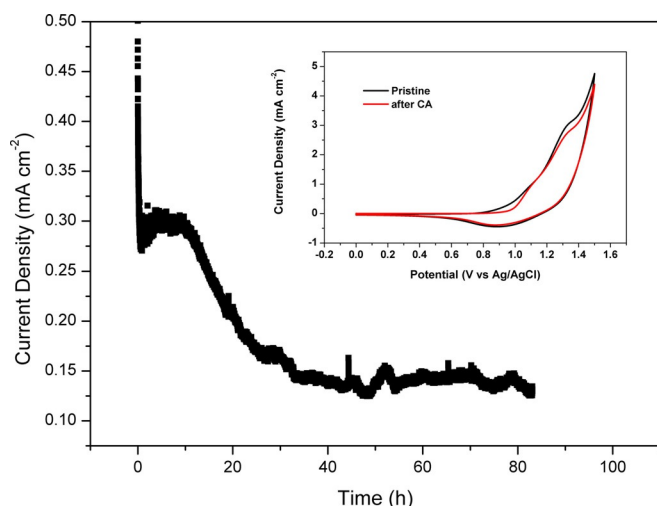


Figure 5. CVs of [Mdca2]-modified FTO electrodes recorded in 50 mM KPi buffer solution with 1 M  $\text{KNO}_3$  as electrolyte at pH 7.0 with a  $50 \text{ mVs}^{-1}$  sweep rate and a blank scan recorded under the same conditions without the catalyst (black line). The arrow shows the scanning direction.

cess was observed at around 1.35 V vs. Ag/AgCl, which can be assigned to the formation of  $\text{Co}^{\text{IV}}$  species.<sup>[20]</sup> The current density in the catalytic region refers only to Faradaic currents as the measured capacitive currents were insignificant (Figure S16). CVs with different scan rates were recorded in the range of 0.5–1.1 V vs. Ag/AgCl to determine the coverage of the redox-active Co centers on the electrode, the so-called surface concentration (Figure S3). The surface concentration ( $\Gamma$ ) was calculated as  $5.80 \text{ nmol cm}^{-2}$  from the slope and is approximately four times higher than that reported for cobalt hexacyanoferrates ( $\Gamma = \sim 1.4 \text{ nmol cm}^{-2}$ ).<sup>[16a]</sup> The relatively high surface concentration of [Codca2] can be explained by a comparison of the distances between the neighboring Co atoms in these systems. The Co sites are much closer to each other in the [Codca2] system ( $\text{Co-Co} = 7.3 \text{ \AA}$ ) than in cobalt hexacyanoferrates ( $\text{Co-Co} \approx 10 \text{ \AA}$ ).

For a detailed assessment of the catalytic activity of the modified electrodes, chronoamperometry measurements were performed at different applied potentials by using a two-compartment cell with a glass frit separator in pH 7.0  $\text{K}_2\text{HPO}_4$  and  $\text{KH}_2\text{PO}_4$  (KPi) buffer solution with 1 M  $\text{KNO}_3$  as the electrolyte. The plot of the logarithm of the steady current densities versus overpotential shows a linear relationship between 323 and 483 mV with a slope of  $94 \text{ mV dec}^{-1}$ . The current density is  $1 \text{ mA cm}^{-2}$  at  $\eta = 580$  mV (Figure S4), whereas it is above 600 mV for cobalt hexacyanoferrates. The improvement in the catalytic performance can be attributed to the increase in the surface concentration. The surface concentration was also used to compare the TOFs of other non-oxide Co-based systems. A TOF of  $2 \times 10^{-3}$  was obtained at an overpotential of 358 mV (Figure S5), which is higher than that obtained for a cobalt oxide film at pH 7.0 ( $\eta = 410$  mV).<sup>[25]</sup> A self-assembled  $\text{IrO}_2$  colloid on an FTO electrode and an electrodeposited  $\text{IrO}_2$ -coated indium tin oxide (ITO) electrode in an aqueous medium were reported have TOF values of  $2.3 \times 10^4$  (pH 5.3) and  $1.64 \times 10^4 \text{ h}^{-1}$  (pH 6.3) at 1.3 V vs. Ag/AgCl, respectively, whereas a TOF value of  $2.00 \times 10^4 \text{ h}^{-1}$  (pH 7) for [Codca2] was obtained under the same potentiostatic conditions.<sup>[26]</sup>



**Figure 6.** Current profile of long-term electrolysis performed for 6 days at 1.2 V (vs. Ag/AgCl) at pH 7.0 of a [Codca2]-modified electrode.

The stability of [Codca2] was tested over approximately six days by using chronoamperometry under same experimental conditions at 1.2 V vs. Ag/AgCl (Figure 6). During this period, electrolysis was performed for four days without interruption and then continued for two more days. The current density decreases until approximately 1 h and then it increases for a short period, probably because of the change in the morphology of the electrode surface, which leads to a change in the surface concentration. Upon further electrolysis, the current density decreases until it stabilizes at around  $0.15 \text{ mA cm}^{-2}$  after 144 h, which implies the stable performance of [Codca2] during water electrolysis and the lack of degradation of the FTO electrode surface. Furthermore, CVs recorded before and after the long-term stability measurement show a similar behavior, which verifies the stability of [Codca2] (Figure 6, inset). Moreover, the stability of [Codca2] was investigated in acidic and basic media. The Pourbaix diagram obtained by performing CVs at different pH values shows that the  $\text{Co}^{2+/3+}$  and  $\text{Co}^{3+/4+}$  redox bands shift to higher potentials gradually as the pH decreases (Figure 7). CVs recorded at different pH values also show that current density obtained at high anodic potentials increases significantly with an increase of the pH, which is expected from the electrocatalytic water oxidation process that involves proton-coupled electron transfer (Figure S6).

The Faradaic efficiency of the process was evaluated by using bulk electrolysis for 3 h.  $\text{O}_2$  evolution was measured by using an oxygen-sensing instrument and compared with the theoretical amount calculated from Faraday's law for a  $4e^-$  redox process (Figure 8). The amount of dissolved  $\text{O}_2$  molecules detected during bulk electrolysis matches the theoretical amount of evolved  $\text{O}_2$  with an efficiency of 100%. This confirms that no competing redox reactions take place and that the current density is quantitative for oxygen production.

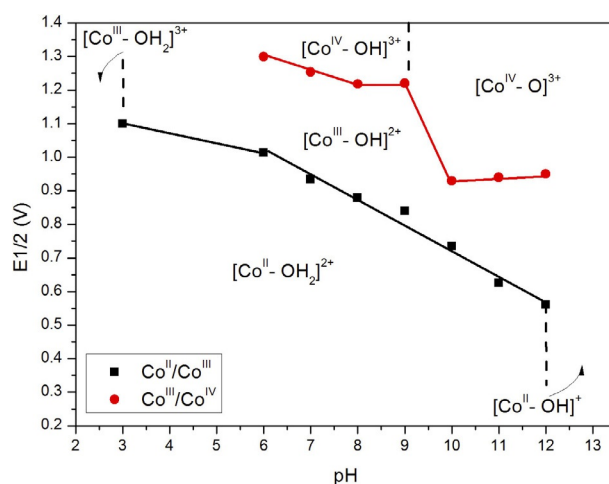


**Figure 7.** Pourbaix diagram that shows the pH/potential characteristics of the precatalytic features of the [Codca2] system. The features denoted as ■ represent the first precatalytic feature, whereas those represented as ● refer to the second precatalytic feature. As reduction bands are not observed particularly in the acidic region and for the second precatalytic features,  $E_{1/2}$  values are estimated from the midpoint of the oxidation bands.

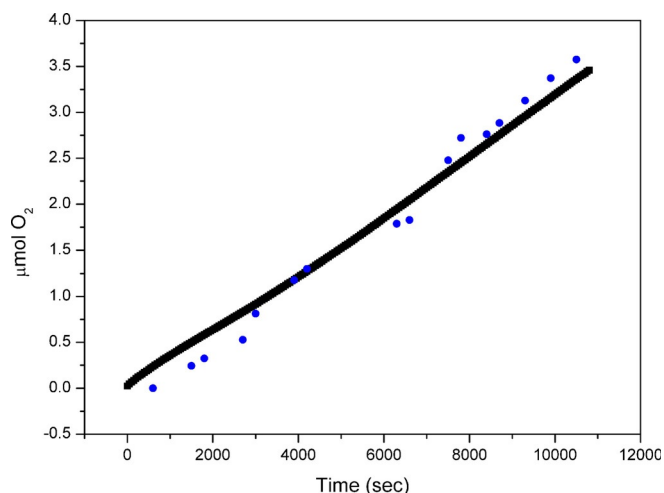


**Figure 8.** Catalytic oxygen evolution recorded (blue) during bulk electrolysis by using an oxygen-sensing probe and theoretical plot assuming Faradaic behavior (black).

### Characterization of electrodes

X-ray photoelectron spectroscopy (XPS) was performed on the electrodes before (pristine electrode) and after the bulk electrolysis (postcatalytic electrode; Figure 9) to study possible changes in the oxidation state and the composition of [Codca2]. The  $\text{Co} 2p_{3/2}$  signal at a binding energy (BE) of 782.78 eV and that of  $\text{Co} 2p_{1/2}$  at BE = 798.78 eV were observed as broad peaks with a high full width at half maximum (FWHM;  $> 4 \text{ eV}$ ) in the pristine electrode, which corresponds well with standard  $\text{Co}^{\text{II}}$  (BE = 782.28 and 798.38 eV, respectively).<sup>[27]</sup> Additionally, scalable satellite bands were observed 4–8 eV above the principle signals. The postcatalytic electrode exhibits a slight shift to lower binding energies ( $\sim 2.5 \text{ eV}$ ) with a  $\text{Co} 2p_{3/2}$  signal at BE = 780.48 eV and a  $\text{Co} 2p_{1/2}$  signal at BE =

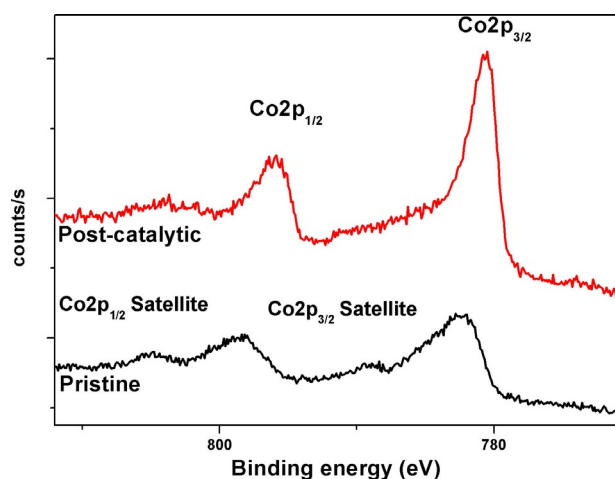


**Figure 9.** XPS spectra of the Co 2p region of the surface of the pristine and postcatalytic electrodes.

795.88 eV<sup>[28]</sup> The signals are relatively sharper with a lower FWHM (~3 eV), and the satellite bands, though identifiable, are less distinctive. Earlier studies reported that these changes can be attributed to the partial oxidation of the surface metal sites.<sup>[19]</sup> FTIR spectra of the pristine and postcatalytic electrodes show no visible changes that can be attributed to structural or compositional changes in the catalyst. Hence, the partial oxidation of the surface Co sites is not permanent and is reversible.<sup>[19]</sup>

Furthermore, the XPS O 1s signals of the pristine and postcatalytic samples were analyzed to study the nature of the partial oxidation (Figure S7). The O 1s signal at a BE higher than 530 eV corresponds to oxygen species such as  $-\text{OH}$ <sup>[29]</sup> adsorbed onto the surface of the catalyst, which indicates the absence of Co–O species during the course of the electrolysis.<sup>[17]</sup> The slight shift in the O 1s position and the relatively higher intensity can be attributed to the partial replacement of DMF on the surface with water because of their miscibility. Moreover, grazing-incidence X-ray diffraction (GI-XRD) analysis of the pristine and postcatalytic electrodes (Figure S17) reveals that there is no distinguishable change in the crystalline phase of [Codca2]. Hence it can be concluded that no cobalt oxides are formed, which confirms that the partial oxidation of surface Co sites is not permanent.

### Metal-doped cobalt dicyanamides

The introduction of a secondary metal ion such as Ni by the partial substitution of metal sites to Co-based heterogeneous WOCs has been studied previously for both oxide and non-oxide systems to enhance the water-oxidation performance of the catalysts.<sup>[30]</sup> This strategy has also been employed for the catalysts studied here, not only to obtain a detailed map of the catalytic performances of mixed-metal dicyanamides but also to investigate the origin of the effect of doping on the catalytic activity. Five mixed-metal dicyanamides with different stoichiometric ratios of Co, Fe, and Ni, which are formulated as  $\text{Co}_{0.5}\text{Ni}_{0.5}(\text{dca})_2(\text{dmf})_2$ ,  $\text{Co}_{0.5}\text{Fe}_{0.5}(\text{dca})_2(\text{dmf})_2$ ,  $\text{Co}_{0.9}\text{Ni}_{0.1}(\text{dca})_2(\text{dmf})_2$ ,

$\text{Co}_{0.9}\text{Fe}_{0.1}(\text{dca})_2(\text{dmf})_2$ , and  $\text{Co}_{0.9}\text{Ni}_{0.05}\text{Fe}_{0.05}(\text{dca})_2(\text{dmf})_2$ , were synthesized using the same synthetic protocol applied for [Mdca2] (Co, Ni, and Fe). The compounds were characterized by using XRD and IR spectroscopy, which showed that the compounds are isostructural (Figures S8–S9).

The current densities of eight compounds were recorded after 600 s under an applied potential of 1.2 V. The data are represented in the contour plot displayed in Figure 10. Relatively lower current densities are obtained for the Fe derivatives (Figure S10). The contour plot exhibits the highest current

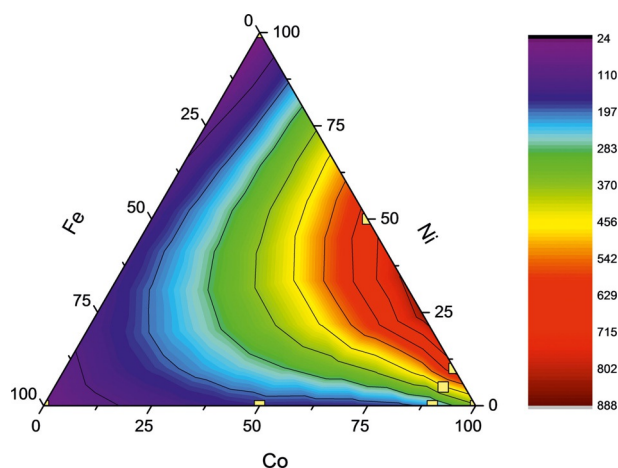


**Figure 10.** Contour plots of the current densities of the eight metal dicyanamide derivatives.

density if the Ni concentration is supported at 10–50% for binary compounds, whereas [Nidca2] exhibits lower current densities than [Codca2] and the mixed Co/Ni derivatives. CVs of the Co/Ni dicyanamides show a similar trend in which  $[\text{Co}_{0.9}\text{Ni}_{0.1}\text{dca2}]$  exhibits the highest current at high anodic potentials (Figure 11). Moreover, chronoamperometric studies performed on the derivatives indicate that all three catalysts have similar Tafel slopes, and the best catalytic performance is

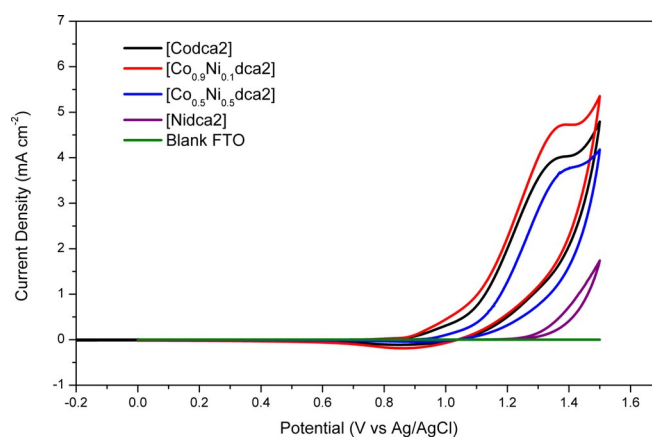


**Figure 11.** Cyclic voltammograms of [Codca2], [Nidca2],  $[\text{Co}_{0.9}\text{Ni}_{0.1}\text{dca2}]$ , and  $[\text{Co}_{0.5}\text{Ni}_{0.5}\text{dca2}]$  recorded in 50 mM KPi buffer solution with 1 M  $\text{KNO}_3$  as electrolyte at pH 7.0 with a  $50 \text{ mV s}^{-1}$  sweep rate and a blank scan recorded under the same conditions without the catalyst (green line).

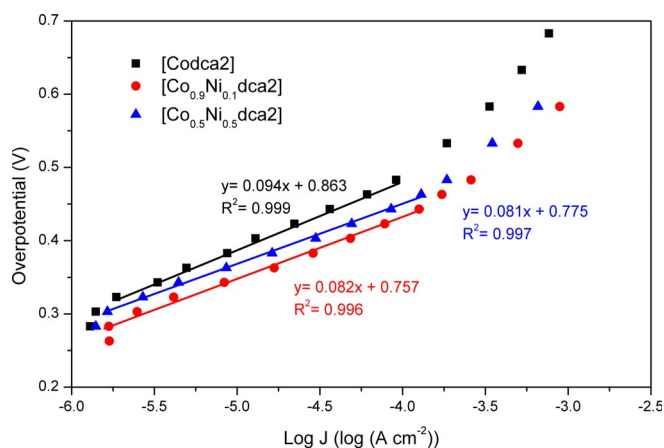


**Figure 12.** Tafel plots obtained for [Codca2] (black), [Co<sub>0.9</sub>Ni<sub>0.1</sub>dca2] (red), and [Co<sub>0.5</sub>Ni<sub>0.5</sub>dca2] (blue). Measurements performed in 50 m KPi buffer solution with 1 m KNO<sub>3</sub> as electrolyte.

observed for [Co<sub>0.9</sub>Ni<sub>0.1</sub>dca2] (Figure 12). A current density of 1 mAcm<sup>-2</sup> can be achieved only with an overpotential of 511 mV for [Co<sub>0.9</sub>Ni<sub>0.1</sub>dca2], whereas it is 580 mV for [Codca2]. Even though the comparison of the catalytic activities of [Codca2] and [Nidca2] indicates clearly that Co sites serve as better catalytic sites than Ni ones, the partial substitution of Co atoms with Ni leads to an increase in the catalytic activity.

The unexpected improvement in the catalytic activity can be well correlated with surface concentrations of catalysts that are obtained by performing CV on the Co<sup>2+</sup>/Co<sup>3+</sup> band at different scan rates (Table 1 and Figure S11). The change of TOF with respect to the overpotential is almost identical, which suggests that the origin of the catalytic activity is the same active site and that the partial substitution of Co sites with Ni ions has a significant effect on the morphology of the catalyst and, thus, on the number of electroactive Co sites on the surface (Figure S12).

**Table 1.** Structural parameters of the catalysts.

M(dca) <sub>2</sub> (dmf) <sub>2</sub>	Surface concentration [nmol cm <sup>-2</sup> ]	S <sub>BET</sub> [m <sup>2</sup> g <sup>-1</sup> ]	Pore size [Å]	Crystallite Size [Å]
[Codca2]	5.80	2.0	98.9–298.79	> 1000
[Co <sub>0.9</sub> Ni <sub>0.1</sub> dca2]	6.64	10.2	157.525–230.178	602
[Co <sub>0.5</sub> Ni <sub>0.5</sub> dca2]	4.74	50.9	110.392–166.27	584

Detailed structural characterization and electrochemical studies were performed on [Codca2], [Co<sub>0.5</sub>Ni<sub>0.5</sub>dca2], and [Co<sub>0.9</sub>Ni<sub>0.1</sub>dca2] to investigate the effect of partial addition of nickel to the microstructure of the samples. The compositions of these clusters were confirmed by using energy-dispersive X-ray (EDX) analysis (Table S3). XRD patterns indicate that all of the compounds are isostructural, and a broadening is observed as the amount of Ni increases, which can be attributed to a decrease in the degree of crystallinity. An estimation of the crystallite sizes by applying the Scherrer formula shows that the

crystallite sizes decrease to 602 and 584 Å, respectively, for [Co<sub>0.9</sub>Ni<sub>0.1</sub>dca2] and [Co<sub>0.5</sub>Ni<sub>0.5</sub>dca2] compared to that of [Codca2] (> 1000 Å). SEM images obtained for the clusters (Figure S13) show a significant change in the morphology of the particles with the addition of Ni. These three compounds were also characterized by using N<sub>2</sub> sorption analysis to deduce the surface area. The samples were subjected to BET surface area measurements by studying the N<sub>2</sub> adsorption and desorption isotherms at 77 K (Figures S14 and S15). All of the samples appear to exhibit mesoporous behavior with varying surface areas. [Codca2] appears to have the lowest surface area, whereas [Co<sub>0.5</sub>Ni<sub>0.5</sub>dca2] exhibits a relatively higher surface area with a more uniform porosity, which corresponds well with the crystallite size calculations from the XRD results and the morphological changes observed by using SEM. Such a correlation was not achieved for the Fe derivatives because of their hygroscopic nature, which is confirmed by using FTIR spectroscopy and SEM. Overall, the study shows clearly that the addition of Ni sites to cobalt dicyanamide leads to an increase in the surface area and the number of metal atoms on the surface, however, with the expense of substituting some of the electroactive Co sites with less active Ni sites. The highest surface concentration was obtained for [Co<sub>0.9</sub>Ni<sub>0.1</sub>dca2], although the highest surface area was achieved for [Co<sub>0.5</sub>Ni<sub>0.5</sub>dca2].

## Conclusions

Recently, the investigation of new non-oxide heterogeneous water-oxidation catalysts has become a growing theme as research on both single Co complexes with pyridil groups and cyanide-based systems show that {CoN<sub>6</sub>} matrices have better turnover frequencies (TOFs) than {CoO<sub>6</sub>} ones. Heterogeneous systems based on cyanide and cyanamide bridging groups have been reported recently. In this study, a new family of 1D coordination compounds with dicyanamide bridging groups was reported. Single-crystal and powder XRD studies indicate that all compounds, Co, Fe, and Ni derivatives and mixed-metal dicyanamides, reported in this study are isostructural.

Cobalt dicyanamides are efficient water-oxidation catalysts with a TOF value of 2 × 10<sup>-3</sup> at η = 358 mV, and an overpotential of only 580 mV is required to produce a current density of 1 mAcm<sup>-2</sup>. This overpotential could further be reduced to 510 mV by introducing 10% Ni impurities. The catalyst of interest is robust in a wide pH range (3.0–12.0). It also retains its structural integrity during long-term catalytic tests (70 h).

We have shown that the estimation of surface concentration using the slope of the linear fit between the peak currents and scan rate is a viable method that could correlate the catalytic performance of compounds with identical crystalline structures.

In summary, the rich and diverse chemistry of metal dicyanamides has promising applications in the field of water oxidation. They have several key advantages as water-oxidation catalysts: i) they have relatively high surface active sites, ii) they have higher TOFs than cobalt oxides, iii) they are robust at high anodic potentials and in acidic and basic media, and iv) the structure of the final product is highly sensitive to the

synthetic protocol, which enables the easy tuning of the structure. Our preliminary studies show that cobalt dicyanamides with different crystal structures could be prepared by using different solvents during synthesis. Such flexibility in the synthesis will be used in the future to establish a correlation with the structure and catalytic application by a systematic investigation of the catalytic activities of similar cobalt dicyanamides.

## Experimental Section

Co(NO<sub>3</sub>)<sub>2</sub>·6H<sub>2</sub>O, FeSO<sub>4</sub>·7H<sub>2</sub>O, Ni(NO<sub>3</sub>)<sub>2</sub>·6H<sub>2</sub>O, NaN(CN)<sub>2</sub>, and all the solvents were of analytical grade, procured from Sigma–Aldrich, and used without any further processing. Millipore deionized water (resistivity: 18 mΩ cm<sup>-1</sup>) was used for all the experiments.

Typically, dicyanamide solution in DMF was added slowly to metal salt in water under constant stirring in a stoichiometric ratio of 2:1 (dca/metal).<sup>[24]</sup> The resulting pink suspension was stirred overnight followed by filtration using suction. The collected precipitate was then washed several times with water/methanol and dried overnight in the oven at 60 °C. IR:  $\tilde{\nu}$  = 2979(w), 2925(w), 2333(m), 2247(sh), 2184(vs), 1236(m), 932 cm<sup>-1</sup> (m).

## Instrumentation

Elemental analyses were performed by using a Thermo Scientific FLASH 2000 CHNS/O analyzer. FTIR spectra were measured by using a Bruker ALPHA Platinum-ATR spectrometer in the wave number range 4000–400 cm<sup>-1</sup>. XRD patterns were recorded by using a Panalytical X'PertPro Multipurpose X-Ray Diffractometer (MPD) employing CuK<sub>α</sub> X-ray radiation ( $\lambda$  = 1.5418 Å). GI-XRD patterns were recorded by using a Panalytical X'Pert<sup>3</sup> MRD Material Research Diffractometer (MRD) employing CuK<sub>α</sub> X-ray radiation ( $\lambda$  = 1.5418 Å) at an incident ( $w$ ) angle of 0.5°. Single-crystal XRD was performed by using a Rigaku MicroMax 007HF model equipped with monochromatic MoK<sub>α</sub> radiation. SEM imaging was performed at beam voltage 5 kV, and EDX analysis was performed at 30 kV by using a FEI-Quanta 200 FEG ESEM. XPS studies were performed by using a Thermo Scientific K-Alpha X-Ray Photoelectron Spectrometer system operated with a AlK<sub>α</sub> microfocused monochromator source ( $h\nu$  = 1486.6 eV, 400 mm spot size) along with a flood gun for charge neutralization, a pass energy of 200 eV was used for the survey scan and 30 eV was used for individual element scans. A Micromeritics Tristar 3000 surface area and porosity analyzer was used to perform N<sub>2</sub> adsorption studies at 77 K to obtain the surface area. Origin Pro 8.5 was used to plot and analyze all of the graphs.

## Preparation of catalyst-modified electrodes

FTO electrodes (1 × 2 cm, 2 mm slides with 7 Ω sq<sup>-1</sup> surface resistivity and ~80% transmittance) were washed by sonication for 10 min in basic soapy solution, deionized water, and isopropanol followed by annealing at 400 °C for 30 min. The catalyst was coated onto the FTO electrode by a drop-casting method. A mixture of 5 mg catalyst, 500 μL water, 500 μL DMF, and 20 μL Nafion was sonicated for 30 min to make a stable suspension. Then, 50 μL of the sonicated suspension of the catalyst was then dropped onto a clean FTO electrode (1 cm<sup>2</sup>). The electrode was then dried in an oven at 80 °C for 10 min and left under desiccation until further use for CV and bulk electrolysis studies. The electrode was rinsed with deionized water before use.

## Electrochemical studies

Electrochemical experiments were performed at RT by using a Gamry Instruments Interface 1000 Potentiostat/Galvanostat. A conventional three-electrode electrochemical cell was used with a Ag/AgCl electrode (3.5 M KCl) as the reference electrode, Pt wire as the counter electrode, and FTO as the working electrode. Before the preparation of an electrode, FTO slides were cleaned described previously.<sup>[16a]</sup> Buffer solutions were prepared using K<sub>2</sub>HPO<sub>4</sub> and KH<sub>2</sub>PO<sub>4</sub> (KPi) and then adjusted by adding H<sub>3</sub>PO<sub>4</sub> or KOH to obtain the desired pH. CVs were recorded with a scan rate of 50 mV s<sup>-1</sup> in 50 mM KPi (pH 7) that contained 1 M KNO<sub>3</sub> as the electrolyte between 0 and 1.5 V (vs. Ag/AgCl). For double-layer capacitance determinations, the scan rate was varied between 10 and 300 mV s<sup>-1</sup> over a small window in which no Faradaic current was observed. The electrochemical double-layer capacitance ( $C_{DL}$ ) was extracted from  $i_c = \nu \times C_{DL}$  in which  $\nu$  is the scan rate and  $i_c$  is the current density for the specific curve at 0.15 V. All experiments were performed under a N<sub>2</sub> atmosphere.

## Bulk water electrolysis and Tafel analysis

Bulk water electrolysis studies were performed by using a two-compartment cell with a glass frit separator. The Pt wire counter electrode was placed in one compartment, and the FTO working electrode and Ag/AgCl reference electrode were placed in the other compartment. The electrolysis experiments were performed in KPi buffer (pH 7.0) solution that contained 1 M KNO<sub>3</sub> as the supporting electrolyte. Tafel data were collected under the same conditions at different applied potentials using the steady current density of an equilibrium time of 600 s. Oxygen evolution was determined by using a YSI 5100 oxygen-sensing instrument equipped with a dissolved oxygen field probe inserted into the anodic compartment.

## Acknowledgements

The authors thank the Science and Technology Council of Turkey, TUBITAK (Project No: 114Z473) for financial support. A.T.B. thanks TUBITAK (2210-C) for the scholarship. E.U. thanks TUBITAK for support (Project No: 1929B011500059).

**Keywords:** amides • cobalt • electrochemistry • n ligands • water splitting

- [1] a) J. Goldemberg, *Science* **1995**, *269*, 1058–1059; b) N. S. Lewis, D. G. Nocera, *Proc. Natl. Acad. Sci. USA* **2006**, *103*, 15729–15735; c) M. Hoel, S. Kverndokk, *Resour. Energy Econ.* **1996**, *18*, 115–136; d) M. Höök, X. Tang, *Energy Policy* **2013**, *52*, 797–809.
- [2] a) M. I. Hoffert, K. Caldeira, A. K. Jain, E. F. Haites, L. D. D. Harvey, S. D. Potter, M. E. Schlesinger, S. H. Schneider, R. G. Watts, T. M. L. Wigley, D. J. Wuebbles, *Nature* **1998**, *395*, 881–884; b) T. M. L. Wigley, R. Richels, J. A. Edmonds, *Nature* **1996**, *379*, 240–243; c) A. K. Jain, H. S. Kheshgi, M. I. Hoffert, D. J. Wuebbles, *Global Biogeochem. Cycles* **1995**, *9*, 153–166; d) S. H. Schneider, L. H. Goulder, *Nature* **1997**, *389*, 13–14; e) C. Withagen, *Resour. Energy Econ.* **1994**, *16*, 235–242.
- [3] S. Chu, A. Majumdar, *Nature* **2012**, *488*, 294–303.
- [4] D. J. Durbin, C. Malardier-Jugroot, *Int. J. Hydrogen Energy* **2013**, *38*, 14595–14617.
- [5] L. Schlapbach, A. Züttel, *Nature* **2001**, *414*, 353–358.
- [6] P. F. Smith, L. Hunt, A. B. Laursen, V. Sagar, S. Kaushik, K. U. D. Calvinho, G. Marotta, E. Mosconi, F. De Angelis, G. C. Dismukes, *J. Am. Chem. Soc.* **2015**, *137*, 15460–15468.

- [7] a) J. Barber, *Chem. Soc. Rev.* **2009**, *38*, 185–196; b) W. Wang, Z. Wang, Q. Zhu, G. Han, C. Ding, J. Chen, J.-R. Shen, C. Li, *Chem. Commun.* **2015**, *51*, 16952–16955.
- [8] a) D. G. Nocera, *Acc. Chem. Res.* **2012**, *45*, 767–776; b) K. N. Ferreira, T. M. Iverson, K. Maghlaoui, J. Barber, S. Iwata, *Science* **2004**, *303*, 1831–1838; c) G. Ananyev, L. Zaltsman, C. Vasko, G. Dismukes, *Biochim. Biophys. Acta Bioenerg.* **2001**, *1503*, 52–68.
- [9] a) D. K. Dogutan, J. R. McGuire, D. G. Nocera, *J. Am. Chem. Soc.* **2011**, *133*, 9178–9180; b) K. M. Macounová, N. Simic, E. Ahlberg, P. Krtil, *J. Am. Chem. Soc.* **2015**, *137*, 7262–7265.
- [10] a) Y. Gao, X. Ding, J. Liu, L. Wang, Z. Lu, L. Li, L. Sun, *J. Am. Chem. Soc.* **2013**, *135*, 4219–4222; b) A. A. Ismail, D. W. Bahnemann, *Sol. Energy Mater. Sol. Cells* **2014**, *128*, 85–101.
- [11] a) K. Maeda, *J. Photochem. Photobiol. C* **2011**, *12*, 237–268; b) D. J. Martin, P. J. T. Reardon, S. J. A. Moniz, J. Tang, *J. Am. Chem. Soc.* **2014**, *136*, 12568–12571.
- [12] a) M. D. Symes, D. A. Lutterman, T. S. Teets, B. L. Anderson, J. J. Breen, D. G. Nocera, *ChemSusChem* **2013**, *6*, 65–69; b) A. M. Ullman, C. N. Brodsky, N. Li, S.-L. Zheng, D. G. Nocera, *J. Am. Chem. Soc.* **2016**, *138*, 4229–4236.
- [13] a) K. Meyer, M. Ranocchiari, J. A. van Bokhoven, *Energy Environ. Sci.* **2015**, *8*, 1923–1937; b) B. You, N. Jiang, M. Sheng, S. Gul, J. Yano, Y. Sun, *Chem. Mater.* **2015**, *27*, 7636–7642.
- [14] a) F. He, F. Li, *Energy Environ. Sci.* **2015**, *8*, 535–539; b) Gurudayal, D. Sabba, M. H. Kumar, L. H. Wong, J. Barber, M. Grätzel, N. Mathews, *Nano Lett.* **2015**, *15*, 3833–3839.
- [15] B. Li, F. Li, S. Bai, Z. Wang, L. Sun, Q. Yang, C. Li, *Energy Environ. Sci.* **2012**, *5*, 8229–8233.
- [16] a) S. Pintado, S. Goberna-Ferrón, E. C. Escudero-Adán, J. R. Galán-Mascarós, *J. Am. Chem. Soc.* **2013**, *135*, 13270–13273; b) S. Goberna-Ferrón, W. Y. Hernández, B. Rodríguez-García, J. R. Galán-Mascarós, *ACS Catal.* **2014**, *4*, 1637–1641; c) H. T. Bui, D. Y. Ahn, N. K. Shrestha, M. M. Sung, J. K. Lee, S.-H. Han, *J. Mater. Chem. A* **2016**, *4*, 9781–9788.
- [17] D. Ressnig, M. Shalom, J. Patscheider, R. Moré, F. Evangelisti, M. Antonietti, G. R. Patzke, *J. Mater. Chem. A* **2015**, *3*, 5072–5082.
- [18] Y. Yamada, K. Oyama, R. Gates, S. Fukuzumi, *Angew. Chem.* **2015**, *127*, 5705–5709.
- [19] M. Aksoy, S. V. K. Nune, F. Karadas, *Inorg. Chem.* **2016**, *55*, 4301–4307.
- [20] a) D. J. Wasylenko, R. D. Palmer, E. Schott, C. P. Berlinguette, *Chem. Commun.* **2012**, *48*, 2107–2109; b) D. J. Wasylenko, C. Ganesamoorthy, J. Borau-Garcia, C. P. Berlinguette, *Chem. Commun.* **2011**, *47*, 4249–4251.
- [21] a) D. Mal, R. Sen, E. Rentschler, K. Okamoto, Y. Miyashita, S. Koner, *Inorg. Chim. Acta* **2012**, *385*, 27–30; b) J. L. Manson, D. W. Lee, A. L. Rheingold, J. S. Miller, *Inorg. Chem.* **1998**, *37*, 5966–5967; c) J. L. Manson, C. R. Kmety, Q. Huang, J. W. Lynn, G. M. Bendele, S. Pagola, P. W. Stephens, L. M. Liable-Sands, A. L. Rheingold, A. J. Epstein, *Chem. Mater.* **1998**, *10*, 2552–2560; d) J. W. Raebiger, J. L. Manson, R. D. Sommer, U. Geiser, A. L. Rheingold, J. S. Miller, *Inorg. Chem.* **2001**, *40*, 2578–2581.
- [22] a) D. Rajan, P. A. Quintero, K. A. Abboud, M. W. Meisel, D. R. Talham, *Polyhedron* **2013**, *66*, 142–146; b) J. L. Manson, A. M. Arif, C. D. Incarvito, L. M. Liable-Sands, A. L. Rheingold, J. S. Miller, *J. Solid State Chem.* **1999**, *145*, 369–378.
- [23] a) A. Tekin, O. Karalti, F. Karadas, *Microporous Mesoporous Mater.* **2016**, *228*, 153–157; b) L. Tabrizi, H. Chiniforoshan, P. McArdle, H. Tavakol, B. Rezaei, M. M. Dehcheshmeh, *Polyhedron* **2014**, *69*, 84–89.
- [24] S. R. Batten, P. Jensen, C. J. Kepert, M. Kurmoo, B. Moubaraki, K. S. Murray, D. J. Price, *J. Chem. Soc. Dalton Trans.* **1999**, 2987–2997.
- [25] Y. Surendranath, M. W. Kanan, D. G. Nocera, *J. Am. Chem. Soc.* **2010**, *132*, 16501–16509.
- [26] a) M. Yagi, E. Tomita, T. Kuwabara, *J. Electroanal. Chem.* **2005**, *579*, 83–88; b) T. Kuwabara, E. Tomita, S. Sakita, D. Hasegawa, A. Koji Sone, M. Yagi, *J. Phys. Chem. C* **2008**, *112*, 3774–3779; c) M. Yagi, E. Tomita, S. Sakita, T. Kuwabara, K. Nagai, *J. Phys. Chem. B* **2005**, *109*, 21489–21491.
- [27] N. S. McIntyre, M. G. Cook, *Anal. Chem.* **1975**, *47*, 2208–2213.
- [28] M. C. Biesinger, B. P. Payne, A. P. Grosvenor, L. W. M. Lau, A. R. Gerson, R. S. C. Smart, *Appl. Surf. Sci.* **2011**, *257*, 2717–2730.
- [29] S. C. Petitto, E. M. Marsh, G. A. Carson, *J. Mol. Catal. A* **2008**, *281*, 49–58.
- [30] X. Zou, J. Su, R. Silva, A. Goswami, B. R. Sathe, T. Asefa, *Chem. Commun.* **2013**, *49*, 7522–7524.

---

 Manuscript received: August 5, 2016

Revised: September 26, 2016

Accepted Article published: October 10, 2016

Final Article published: December 1, 2016